Current Applied Physics 11 (2011) 1192–1196

Contents lists available at ScienceDirect

Current Applied Physics

journal homepage: www.elsevier.com/locate/cap

Control of motion of fullerene colloidals by dielectrophoretic force for electronic paper-like display

Mi-Kyung Kim [a,b], Young Jin Lim [a,b], Surjya Sarathi Bhattacharyya [a,b], Myong-Hoon Lee [a,b], Seung Hee Lee [a,b,*]

[a] Department of BIN Fusion Technology, Chonbuk National University, Jeonju, Jeonbuk 561-756, Republic of Korea
[b] Department of Polymer Nano-Science and Technology, Chonbuk National University, Jeonju, Jeonbuk 561-756, Republic of Korea

ARTICLE INFO

Article history:
Received 4 November 2010
Received in revised form
18 February 2011
Accepted 22 February 2011
Available online 4 March 2011

Keywords:
Fullerene colloidals
Dielectrophoretic force
Electronic paper-like display

ABSTRACT

We have investigated motion of fullerene particles in isotropic and anisotropic dielectric medium for the purpose of application of the particles in electronic paper-like display. The charged particles require higher DC electric field to react in the isotropic silicone oil medium in comparison with anisotropic liquid crystal medium, confirming that the dielectrophoretic force is mainly responsible for the motion of the particles. In addition, we proposed device which can express black, gray and white states with three terminal electrodes by suitable combination of the polarity of applied DC bias field. Finally, our investigation provides the optimization of driving scheme as well as electrode structure.

1. Introduction

The fabrication of information conveying device devoid of space and time limitation is a topic of continuous interest. In realizing such a concept, displays have immense importance as they serve as bridge between human being and information. As electronic paper-like display (EPD) associated with motion of charged particles has the advantages in their usage as plain paper, the said display device is expected to fulfill that purpose in the near future because they exhibit acceptable image quality with bistability. Various EPD modes have been proposed recently, such as in-plane electrophoretic display [1,2], twisting ball display [3], toner display [4,5], electro deposition display [6], microencapsulated electrophoretic display [7–9] etc. Among them the EPD which utilizes dielectrophoretic (DEP) [10–15] method with the help of dispersed particles in the liquid crystal (LC) medium is particularly important because the polarity of LC can be widely controllable, that is, DEP force can be maximized so that very low operating voltage device can be realized. Although the use of dielectrophoresis is rapidly becoming a proven technique for manipulating particles in microfluidic systems but electro-optic (E-O) properties of these devices remain inferior than other displays such as liquid crystal display (LCD) [16–19], organic light-emitting diode (OLED) [20–26], plasma display panel (PDP) [27–29].

The purpose of the present paper is to demonstrate the optimization process of gray scale control in EPD. The simulated distribution of electric field has been demonstrated in the paper and extensively discussed in the paper as electro-optic performance of the device can be anticipated in the said investigation. For experimental verification of the concept C_{60} has been chosen as suspension in clear fluid (Liquid crystal/Silicon oil) and eventually proven its candidature for EPD fabrication. Our paper in addition presents LC medium for the same purpose and shows better electro-optic performance than silicon oil, which might have impact over next generation EPD manufacturing.

2. Experimental conditions and operation concept of the proposed device

The proposed EPD device structure used in the present investigation is depicted in Fig. 1. The bottom glass substrate of the device contains conducting pixel electrodes in the interdigitated structure in which each of them has electrode width (w) of 10 μm and the intra-pixel distances (l) are fixed at 20, 40 and 80 μm, respectively for three distinct cases. The alternative pixels are designated as I and II and they are made of aluminum and indium-tin-oxide (ITO), respectively. The top substrate of the device is made

* Corresponding author. Department of Polymer Nano-Science and Technology, Chonbuk National University, Jeonju, Jeonbuk 561-756, Republic of Korea. Tel.: +82 63 270 2343; fax: +82 63 270 2341.
E-mail address: lsh1@chonbuk.ac.kr (S.H. Lee).

1567-1739/$ – see front matter © 2011 Elsevier B.V. All rights reserved.
doi:10.1016/j.cap.2011.02.018

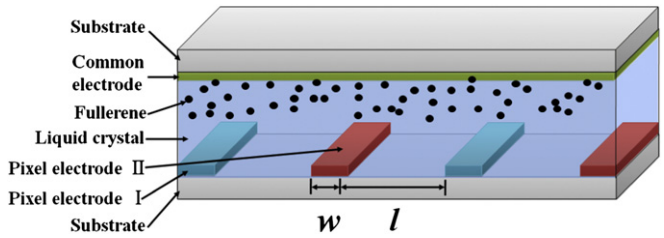

Fig. 1. Schematic diagram of the cell used in the experiment. The pixel electrode I and II are made of aluminum and ITO, fabricated alternatively throughout the bottom substrate for intra-electrode distances (l) 20, 40, 80 μm, respectively, with an electrode width (w) of 10 μm.

of conducting ITO coated glass plate and it serves as common electrode of the said device. For EPD device preparation both the common as well as pixel electrodes has been spin coated to a thickness of 800 Å by a polymer alignment layer of AL-16139 (Japan Synthetic Rubber Co) as an insulation layer. The mechanical rubbing was performed on both substrates along the in-plane field direction for aligning the nematic LC, which minimizes flow motion effect of LC to the C_{60}. The polymer tape is used to maintain a uniform gap d of 60 μm between the electrodes in the assembled cell. In the next step, 10 wt% C_{60} (conductivity ($\sigma_{C_{60}}$) and dielectric permittivity ($\varepsilon'_{C_{60}}$) of $C_{60} \sim 10^{-4}$ S m^{-1} and 6.07, respectively) was mixed into the host nematic LC, purchased from Merck Co. The dielectric anisotropy ($\Delta\varepsilon$) of the LC medium is 7.4 and average dielectric permittivity (ε'_{LC}) = 5.8 at 1 kHz, flow viscosity $\eta = 18$ mm^2/s, $\sigma_{LC} \sim 2.944 \times 10^{-13}$ S m^{-1} at 50 Hz and 25 °C. The mixture was filled into the cell prepared in the previously mentioned method at room temperature by the capillary action technique. Another mixture of 10 wt% C_{60} was prepared using silicone oil as host medium for present investigation. The silicone oil purchased from sigma aldrich with physical properties: dielectric permittivity ($\varepsilon'_{\text{Silicone Oil}}$) = 3.1 at 1 kHz, flow viscosity $\eta = 94.3$ mm^2/s, and $\sigma_{\text{Silicone Oil}} \sim 1.08 \times 10^{-11}$ S m^{-1} at 50 Hz and 25 °C. The photomicrograph of C_{60} mixed LC and silicone oil sample confined in said device has been depicted as insets of Fig. 2 showing homogeneous distribution of C_{60} clusters. The average cluster size distribution as obtained by analyzing several photomicrographs of C_{60} mixed LC and silicone oil sample have also been shown in the same figure. The range of C_{60} cluster size distribution in LC medium ~(3–40 μm) is very wide and broadly peaked in the range of 5–15 μm, whereas that of silicone oil ~(5–30 μm) is much narrow and showing a much sharper peak ~13–15 μm. Hence the occurrence of larger C_{60} clusters is the essential disparity of present isotropic medium in comparison to the anisotropic medium. The

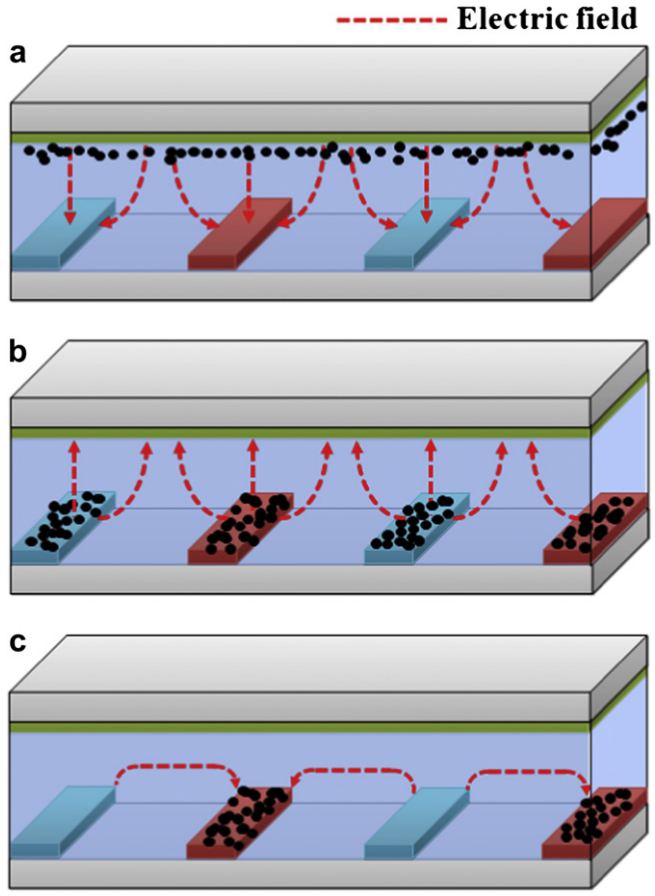

Fig. 3. Schematic diagram of movement of C_{60} in dispersed LC/Silicone oil medium driven by dc: (a) dark state – C_{60} moved toward top common electrode, (b) gray state – C_{60} moved toward bottom pixel electrode I and II, (c) white state – C_{60} moved toward pixel electrode II.

difference in particle size distribution might be attributed to the polar nature of the host LC medium compared to silicone oil. However, the respective frequency of occurrence is peaked around the same cluster size regime (~10–15 μm) for both the medium; indicating most of the C_{60} clusters lie in this regime in both isotropic as well as anisotropic medium.

For driving the device, mentioned pixel electrodes I and II in the interdigited structure are operated by a pair of thin film transistors, formed on them and designated as TFTI and TFTII

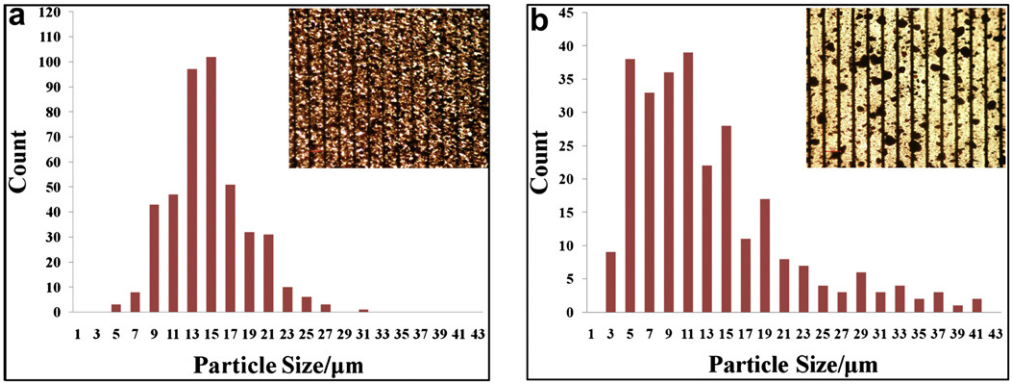

Fig. 2. The cluster size distribution of C_{60} in LC (a) and in silicone oil (b) has been demonstrated as histograms. The photomicrograph of C_{60} dispersed LC and silicone oil has been shown as respective insets.

respectively. The TFTI among the two TFTs is for switching pixel electrode I and TFTII is for switching pixel electrode II. Different voltages can be applied to the pixel electrodes through this method, resulting in dark, gray, white state depending on switching method. The electric field distribution in the present electrode structure has been investigated using the commercially available LCD master (Shintech, Japan) software for understanding the probable dynamics of C_{60} clusters within the device and optimizing the device performance.

3. Results and discussion

The motion of C_{60} particles has been illustrated in Fig. 3, explaining the reaction of the particles to the applied external DC field. In presence of externally applied electric field, C_{60} and the surrounding LC/silicone oil medium are electrically polarized, and surface charge accumulates at the interface due to difference in dielectric permittivity and conductivity. The polarization induces an effective dipole moment on C_{60} and the DEP force arises because of interaction of the particle dipoles and the spatial gradient of the electric field. For an insulating spherical particle of radius 'α', in a non-uniform electric field (E), the net DEP force is given by [30].

$$F_{DEP} = 2\pi\varepsilon'_{medium}\alpha^3 f_{CM}\nabla|E|^2 \quad (1)$$

where, ε'_{medium} represents the dielectric permittivity of the host medium (LC/Silicone oil) and f_{CM} = Clausius-Mossotti (CM) factor, which describes the relaxation in the effective polarizability of the particle

$$f_{CM} = \frac{\sigma_{C_{60}} - \sigma_{LC/Silicon\_Oil}}{\sigma_{C_{60}} + \sigma_{LC/Silicon\_Oil}} \quad (2)$$

Hence f_{CM} depends on conductivity of C_{60} particles and medium.

Analyzing the effect of F_{DEP} over C_{60} particles in either medium in accordance with Eq. 1, the difference in dielectric permittivity of the two medium seems to play the crucial role, as all other parameters are found to be analogous in either medium. The dielectric

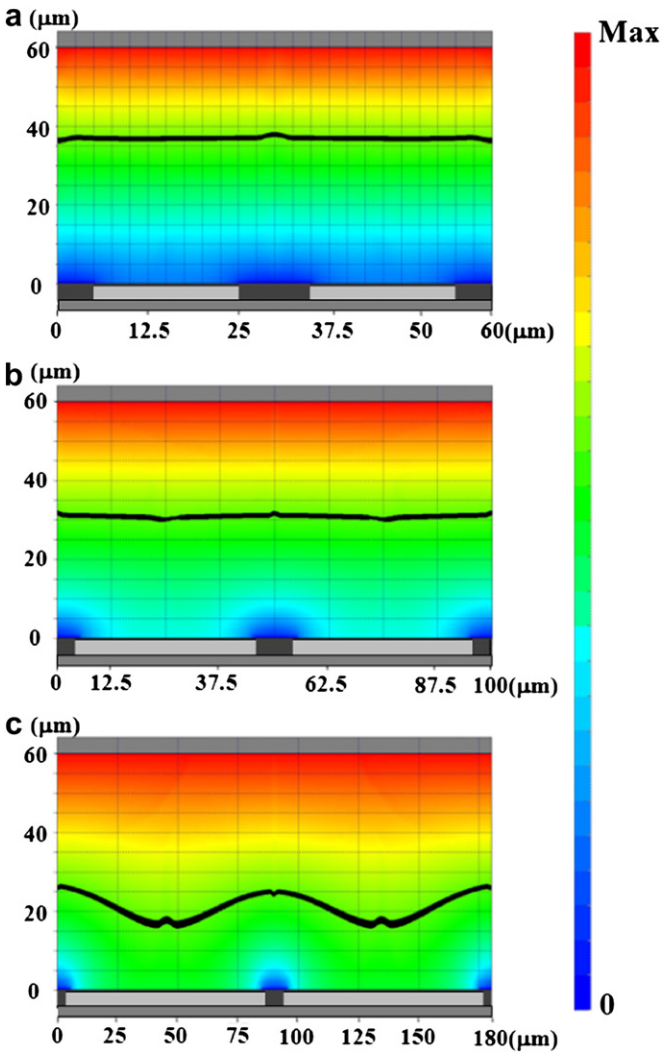

Fig. 4. Side view of vertical electric field strength and equi-potential curves (dark line) in accordance with intra-electrode distance at the dark state. The *x* and *y*-axis represents the electrodes and cell gap, respectively. (a) l = 80 μm, (b) l = 40 μm, (c) l = 20 μm. The continuous increase of electric field strength has been depicted in the figure using the color scale (from blue to red). (For interpretation of the references to color in this figure legend, the reader is referred to the web version of this article.)

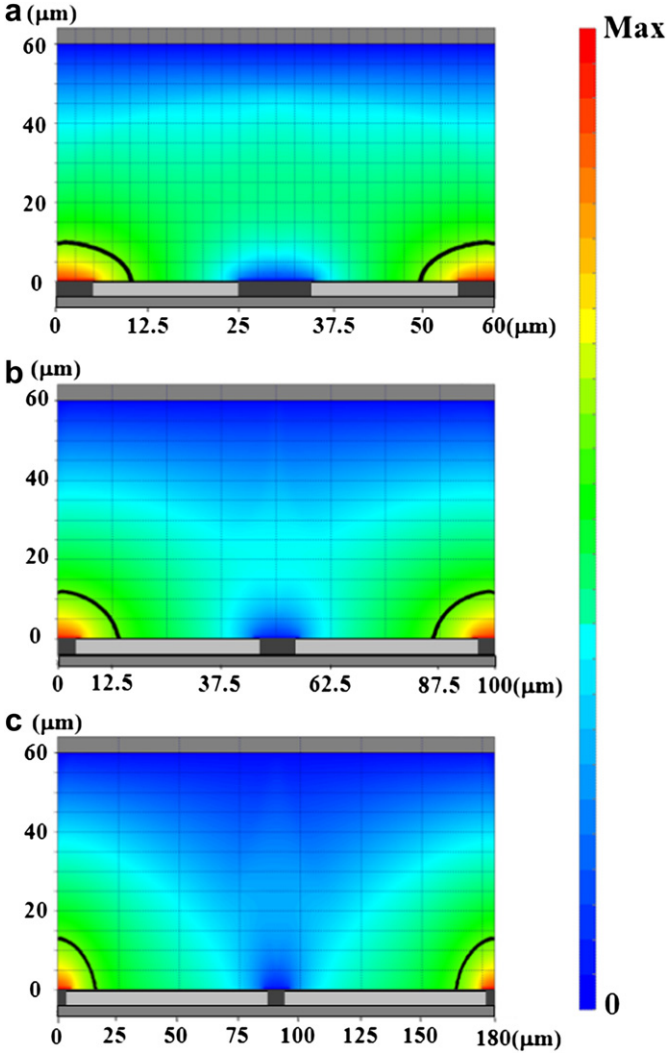

Fig. 5. Side view of horizontal electric field strength and equi-potential curve (dark line) in accordance with intra-electrode distance in the white state. The *x* and *y*-axis represents the electrodes and cell gap, respectively. (a) l = 80 μm, (b) l = 40 μm, (c) l = 20 μm. The continuous increase of electric field strength has been depicted in the figure using the color scale (from blue to red). (For interpretation of the references to color in this figure legend, the reader is referred to the web version of this article.)

permittivity of silicone oil is lesser than that of LC medium, also F_{DEP} is anisotropic due to anisotropic nature of LC medium. Hence F_{DEP} experienced by C_{60} clusters in LC medium seems to be double in magnitude in comparison with that in isotropic silicone oil medium.

The negatively charged C_{60} moves toward the top common electrode driven by DEP force, while DC voltage of positive polarity has been applied there with respect to the bottom pixel electrodes as shown in Fig. 3(a). Hence, an incident light on the device is absorbed by C_{60} particles and thus the device appears to be dark. Gray state is achieved by reversing the polarity of common and pixel electrode, as C_{60} moves in the reverse direction and piles up at pixel electrodes as depicted in Fig. 3(b). Finally, by applying positive polarity of DC voltage to pixel II (made of aluminum or ITO) and negative polarity to pixel I electrode, the mutual attractive as well as repulsive forces insist C_{60} to pile up on pixel II leaving pixel I, so that transmissive or reflective light with a reflector below the bottom substrate can be maximized, resulting in white state.

The predominant components of electric field strength and equi-potential lines are obtained from simulations in distinct steps of device operation and different device structures. The vertical electric field dominates the dark state of the device operation; whereas the white state of the device is dominated by horizontal component of electric field as depicted in Figs. 4 and 5 respectively. The equi-potential curve in respective cell structures has been represented by dark lines. The comparison between Figs. 4 and 5 shows that the electric field intensity at pixel electrode in white state is more than dark sate. This high electric potential in white state induces C_{60} to confine to the alternative ITO made pixels (pixel II). As a result, the substrate area devoid of C_{60} covered pixels transmits the incident visible light through transparent LC medium and generating white state. The variation of electrode gap does not have any significant impact over the equi-potential curves of Fig. 4. The appearance of dark state eliminating white and gray state is attributed to the increased electrical intensity toward the top substrate. Here, the positively polarized electric field is formed at the upper part of the cell gap so that the negatively charged C_{60} move toward the top substrate. Incident visible light failed to penetrate the device, due to indiscriminate dispersion of C_{60} on the top substrate. The vertical electric field between top and bottom substrate occurs evenly in Fig. 4(a) and (b) because intra-electrode region is narrower (20 μm, 40 μm) than cell gap (60 μm). However, the field intensity is found to be weak at the center of intra-electrode region, as the intra-electrode distance is larger (80 μm) than cell gap. Hence, we observed that the electric field strength is evenly distributed between top and bottom substrate in cases of $l = 20$ μm and 40 μm.

The voltage-dependent normalized transmittance curves in accordance with variation of l at gray and white states have been depicted in Fig. 6 for comparative analysis of their electrode structures dependent electro-optic properties using both LC and Silicone oil as dispersive medium. The transmittance of the devices using LC as dispersive medium driven in gray mode Fig. 6(a) with $l = 20$ μm is found to be low as large amount of C_{60} stacks over the intense pixel electrodes, providing very small intra-electrode space for light leakage. However, the transmittance is found to be even lower by increasing l to 80 μm due to significant reduction of electric field strength at the same applied voltage. Appreciably high transmittance is finally obtained by fixing l to 40 μm as in this case the electric field strength is optimum for distribution of C_{60} particles over the pixels as well as providing enough space for light leakage with same driving voltage. However at gray state in identical device structures the change in transmittance of the devices using Silicone oil as dispersive medium is negligible in comparison with the devices using the LC as dispersive medium.

The transmission levels of the white mode of the devices which uses liquid crystal as dispersive medium are found in analogous

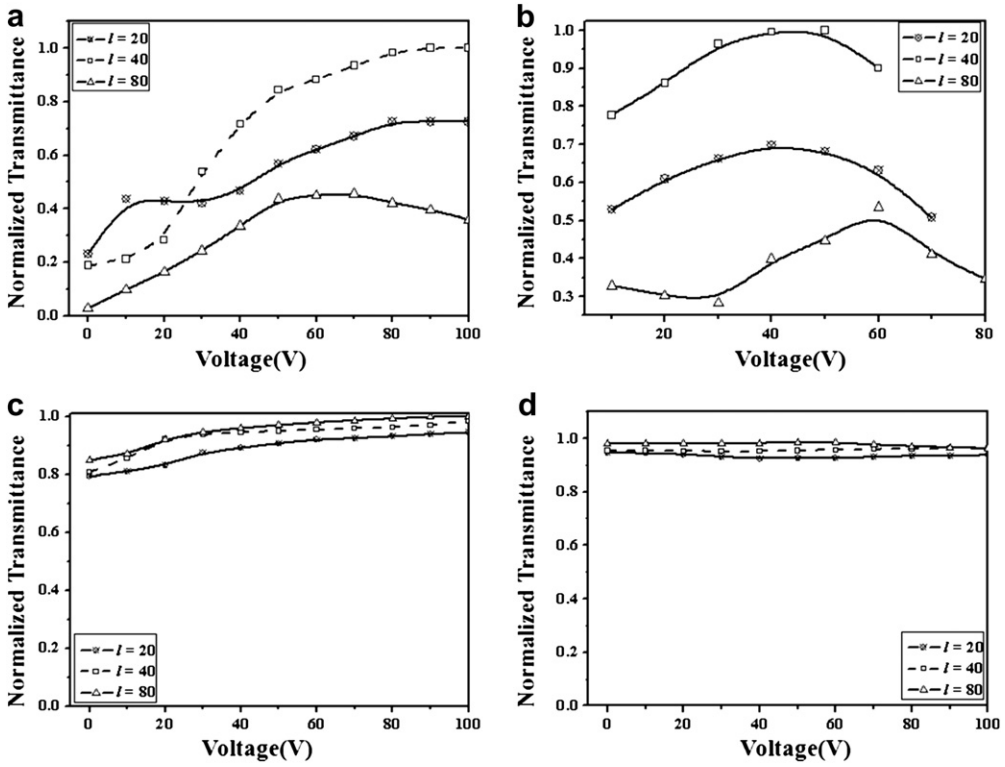

Fig. 6. Comparison of normalized voltage-dependent transmittance curves according to intra-electrode distance at the (a) gray and (b) white states using LC and the (c) gray and (d) white state using Silicon oil as dispersive medium of C_{60}.

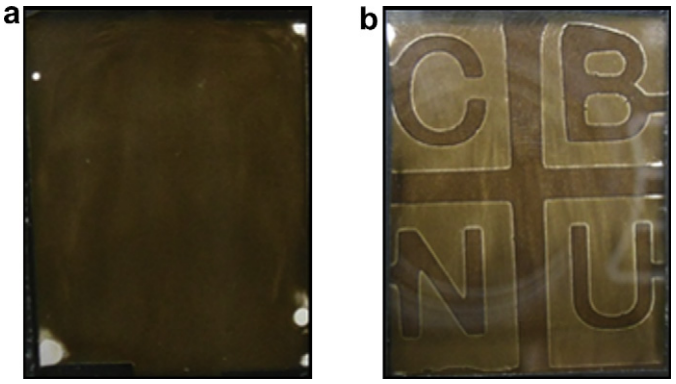

Fig. 7. Images of display made of C_{60} dispersed LC material. The dielectrophoretic force driven display shows: (a) dark image and (b) text image.

order of l, as the transmission level for $l = 40$ μm tops the list followed by $l = 20$ μm and 80 μm cases, due to similar reasons as discussed earlier. The operating voltages of the respective cell structures are found to increase with increasing inter electrode distance. The operating voltage for the device using LC as dispersion medium of C_{60} is 40 V for the case of $l = 20$ μm device, however, it has to be increased to 50 and 60 V respectively for $l = 40$ μm and 80 μm cases. This worth mentioning here that the transmittance level of fabricated similar devices using Silicone oil as dispersion medium instead of LC does not respond to analogous magnitudes of applied voltage.

Hence, our investigation confirms that the driving characteristics transforms according to variation of l. The transmittance increases with increasing l until $l = 40$ μm, but in case of $l = 80$ μm, the transmittance is found to be lower. Similar to the case of gray mode, the reduction of transmittance in case of high l is caused by weaker electric field strength than other cases as driven by the same operating voltage. Additionally, the device shows fairly good electro-optical properties up to reasonable driving voltage when high voltage was applied to solve this problem. However, the electro-optic property degrades when the applied voltage exceeds driving voltage. Therefore, superior electro-optical characteristics are achievable by optimization of electrode structures as well as driving voltage in C_{60}-LC composite system. In the silicone oil medium, however, the movement of C_{60} was different from the LC medium, because F_{DEP} in this medium is much smaller than LC medium due to its lesser dielectric permittivity, also the viscosity of silicone oil medium ($\eta = 94.3$ mm^2/s) was very high in comparison with viscosity of LC medium ($\eta = 18$ mm^2/s).

Fig. 7 shows the formation of a conceptually drawn individual image of a future device made of C_{60}-LC composite. The C_{60} particles are randomly distributed within the cell before applying DC bias and hence, the device does not show any text image as illustrated in Fig. 7(a). When a short electric pulse is applied to the device electrodes, the C_{60} particles start to migrate toward the positive electrodes, which produce a text image as exemplified in Fig. 7(b). When the polarities of electrodes are changed, the C_{60} particles migrate to the opposite direction and create an image with different contrast. Thus C_{60}-LC composite with proper driving scheme, enables manufacturing of EPD device with tunable contrast, which might have future industrial application.

4. Conclusions

We have developed new concept of EPD using C_{60} dispersed LC with dielectrophoretic force to overcome high driving voltage of conventional EPD. The dark, white and gray modes of the device could be realized by DEP force driven movements of C_{60}. The movement of C_{60} molecules in LC medium varies with variation of intra-electrode separation. Tailoring the intra-electrode separation as well as applied DC bias, the transmittance of the device is found to enhance up to a certain limit, however, it tends to decrease while applied voltage becomes too high. The electro-optic characteristics of the devices using anisotropic LC as dispersive medium are found to be superior to the isotropic silicone oil. This investigation confirms certain movement of C_{60} in between different electrodes with variation of voltage and electrode structure and dominance of DEP force in anisotropic LC medium. The reported optimization process of E-O properties regarding driving voltage and pixel structure are the key factors for fabrication of EPD using DEP force driven C_{60} particles. However, further investigation is required to achieve better and better performance either in the form of choice of dispersion medium along with their physical properties (dielectric anisotropy, conductivity etc) as well as the suspending material for achieving the proposed goal.

Acknowledgments

This work was supported by Mid-career Researcher Program through NRF grant funded by the MEST (NO. 2009-008377) and supported by WCU program through MEST (R31-2008-000-20029-0).

References

[1] E. Kishi, Y. Matsuda, Y. Uno, A. Ogawa, T. Goden, N. Ukigaya, M. Nakanishi, T. Ikeda, H. Matsuda, K. Eguchi, SID Int. Symp. Dig. Tech. Pap. 31 (2000) 24.
[2] S.A. Swanson, M.W. Hart, J.G. Gordon II, SID Int. Symp. Dig. Tech. Pap. 31 (2000) 29.
[3] N.K. Sherdon, M.A. Berkovitz, SID Int. Symp. Dig. Tech. Pap. 18 (1977) 289.
[4] G. Jo, K. Sugawara, K. Hoshino, T. Kitamura, IS&T NIP15. International Conference on Digital Printing Technologies (1999) p. 590.
[5] K. Shigehiro, Y. Yamaguchi, Y. Machida, M. Sakamaki, T. Matsunaga, Proc. Jpn. Hardcopy 2001 (2001) p. 135.
[6] K. Shinozaki, SID Int. Symp. Dig. Tech. Pap. 33 (2002) 39.
[7] B. Comiskey, J.D. Albert, J. Jacobson, SID Int. Symp. Dig. Tech. Pap. 28 (1997) 75.
[8] B. Comiskey, J.D. Albert, H. Yoshizawa, J. Jacobson, Nature 394 (1998) 253.
[9] H. Kawai, N. Kanae, SID Int. Symp. Dig. Tech. Pap. 30 (1999) 1102.
[10] H.A. Pohl, Dielectrophoresis. Cambridge University Press, Cambridge, England, 1978.
[11] P.J. Bruke, Nanodielectrophoresis: Electronic Nanotweezers, Encyclopedia of Nanoscience and Nanotechnology, vol. 6, American Scientific Publishers, New York, 2003, 623.
[12] T. Bert, H.D. Smet, Displays 24 (2003) 103.
[13] T. Bert, H.D. Smet, Displays 24 (2003) 223.
[14] P. Sureshkumar, A.K. Srivastava, S.J. Jeong, M. Kim, E.M. Jo, S.H. Lee, Y.H. Lee, J. Nanosci. Nanotechnol. 9 (2009) 4741.
[15] A.K. Srivastava, M. Kim, S.M. Kim, M.-K. Kim, K. Lee, Y.H. Lee, M.H. Lee, S.H. Lee, Phys. Rev. E 80 (2009) 051702.
[16] M. Oh-E, K. Kondo, Appl. Phys. Lett. 67 (1995) 3895.
[17] S.H. Lee, S.L. Lee, H.Y. Kim, Appl. Phys. Lett. 73 (1998) 2881.
[18] J.W. Park, Y.J. Ahn, J.H. Jung, S.H. Lee, R. Lu, H.Y. Kim, S.– T. Wu, Appl. Phys. Lett. 93 (2008) 081103.
[19] A. Takeda, S. Kataoka, T. Sasaki, H. Chida, H. Tsuda, K. Ohmuro, T. Sasabayashi, Y. Koike, K. Okamoto, SID Int. Symp. Dig. Tech. Pap. 29 (1998) 1077.
[20] C.W. Tang, S.A. VanSlyke, Appl. Phys. Lett. 51 (1987) 913.
[21] A.R. Duggal, J.J. Shiang, M.H. Christian, F.F. Donald, Appl. Phys. Lett. 80 (2002) 3470.
[22] B.C. Krummacher, V.-E. Choong, M.K. Mathai, S.A. Choulis, F. So, F. Jermann, T. Fiedler, M. Zachau, Appl. Phys. Lett. 88 (2006) 113506.
[23] S.R. Forrest, Nature 428 (2004) 911.
[24] M.A. Baldo, D.F. O'Brien, Y. You, A. Shoustikov, S. Sibley, M.E. Thompson, S.R. Forrest, Nature 395 (1998) 151.
[25] D.F.O. Brien, M.A. Baldo, M.E. Thompson, S.R. Forrest, Appl. Phys. Lett. 74 (1999) 442.
[26] M.A. Baldo, S. Lamansky, P.E. Burrows, M.E. Thompson, S.R. Forrest, Appl. Phys. Lett. 75 (1999) 4.
[27] S. Cany, J. Kang, C. Punset, J.P. Boeuf, IDW'99 Proceeding (1999) p. 751.
[28] D. Lee, K.Y. Choi, S.C. Choi, D.G. Baek, J.R. Lim, B.N. Ahn, W.B. Park, IMID'07 Technical Digest (2007) p. 123.
[29] D.N. Kim, J.Y. Lee, J.S. Huh, H.S. Kim, J. Non Cryst. Solids 306 (2002) 70.
[30] Y. Kang, D. Li, S.A. Kalams, J.E. Eid, Biomed. Microdevices 10 (2008) 243.